X ECCOMAS Thematic Conference on Smart Structures and Materials
SMART 2023
D.A. Saravanos, A. Benjeddou, N. Chrysochoidis and T. Theodosiou (Eds)

AEROSTRUCTURAL INVESTIGATION OF SHAPE ADAPTIVE ROTOR BLADING FOR THE REDUCTION OF BLI INDUCED LOSSES IN THE DISTORTED FLOW REGIMES OF A TRANSONIC FAN ROTOR

Marcel Seidler*, Jonas Voigt*, Zhuzhell Montano Rejas†, Jens Friedrichs*, Johannes Riemenschneider†, Hans Peter Monner†

*Institute of Jet Propulsion and Turbomachinery
TU Braunschweig
Hermann-Blenk-Straße 37, 38108 Braunschweig, Germany
e-mail: m.seidler@ifas.tu-braunschweig.de

† Institute of Lightweight Systems
German Aerospace Center (DLR)
Lilienthalplatz 7, 38108 Braunschweig, Germany

Key words: Fan Design, Shape-Adaption, Boundary Layer Ingestion

Abstract. Within the Cluster of Excellence for Sustainable and Energy-Efficient Aviation SE^2A, a blended wing body aircraft is investigated to improve efficiency and carbon emissions of future air transport. By embedding the aircraft engines on the top rear fuselage, parts of the aircraft's wing boundary layer are ingested, which has the potential to further improve the engine's propulsion efficiency. Through the ingestion of low momentum fluid however, inflow distortion is induced and the fan rotor operates under increased flow incidence in the distorted flow regimes. To reduce the thereby arising efficiency and pressure ratio penalties in the aircraft engine, alternative design strategies for the fan stage are required. Within this investigation, an active shape morphing mechanism is introduced, which allows to temporarily adjust the fan blading when the fan rotor is exposed to distorted inflow conditions. By integrating piezoceramic actuators into the rotor blading, the blade staggering and turning can be adjusted with the goal to reduce flow incidence and deviation in the distorted flow regimes. For this investigation the NASA rotor 67 is chosen as a reference test case and its performance under boundary layer ingestion (BLI) conditions is evaluated. For the shape morphing assessment, FEA morphing simulations are tightly coupled with a geometry re-engineering methodology and stationary CFD simulations of the actuated fan rotor geometries under distorted inflow. For the chosen test case, the achievable deformations are however too small to compensate for the strong distortion effects of a blended wing body's boundary layer. Therefore, the blade reference design needs to be adapted in order to increase the achievable deformations. This includes the investigation of typical compressor design parameter variations, such as blade hub-to-tip ratio, chord length as well as lean and sweep and their impact on the deformability of a shape-adaptive fan stage.

1 INTRODUCTION

To increase the energy efficiency of future aircraft, new aircraft concepts are investigated. Boundary layer ingestion (BLI) is a promising technology to improve air transport efficiency. Through the ingestion of the aircraft structure's boundary layer, which has a reduced inflow momentum at the engine intake, the propulsion efficiency can be increased [1]. Within the Cluster of Excellence for Sustainable and Energy-Efficient Aviation SE^{2}A, a blended wing body aircraft featuring engines embedded on the top rear fuselage is currently researched (Fig. 2). The ingestion of low momentum fluid leads to distortion effects in the lower shroud area of the intake. The extent of the distorted area is highly depending on the aircraft configuration and therefore the wing design. Together with instationary effects by passing trough areas of different flow conditions, the thereby induced inflow incidence for the fan rotor indicates a major drawback of BLI concepts, as the dominant inflow condition in the distorted area differ from those of the rotor design point. Especially for modern transonic compressor rotors, with an increased tip loading [2], inflow incidence may diminish the BLI benefits through increased losses in the fan stage. To align both BLI effects on the overall propulsion efficiency, this research investigates the concept of a shape-adaptive rotor that allows to morph its shape depending on its circumferential position (Fig. 1, center). While passing the distorted flow regimes, piezoceramic actuators in the rotor blading allow for a specific adaption of the span-wise blade twist and turning, according to the prevalent flow angle variations induced by the low momentum fluid. With the highest achievable deformations located towards the rotor tip [4], the shape-adaption concept increases the design flexibility, where the highest aerodynamic effects of inflow distortion are expected. Based on generic distortion patterns, this research aims to mitigate the drawbacks of inlet distortion through deriving a suitable actuation concept for the distorted flow regimes. For this study, the transonic NASA rotor 67 [3] is transformed into a shape-adaptive system, as previously described by [4]. As the applied piezoceramic Macro Fiber Composite (MFC) actuators allow for actuation frequencies up to 10 kHz [5], an actuation once per rotation is technically feasible for high-speed compressor rotors, such as the chosen test case with a rotational speed of 267 s^{-1} [3]. Modern UHBR turbofans, which would be employed in BLI engines, operate at even lower speeds in the range of 50 s^{-1} [2]. By investigating the effects of BLI on the stage performance, actuation strategies are specified and a structural morphing assessment for different actuation concepts is carried out. To evaluate the potential of the feasible shape variations, representative stationary CFD simulations are conducted for a blade passage with maximum distortion. Finally, a suitable actuation concept is selected and the rotor reference shape is varied to increase its morphing potential and thus its impact on the fan stage performance under distorted inflow conditions. This study therefore combines the comprehensive efforts of the authors to evaluate aerodynamic losses due to boundary layer ingestion [6] with the transformation of conventional compressors into shape-adaptive systems for an increased off-design efficiency.

2 METHODOLOGY

Derivation of distortion pattern: To generate an authentic BLI distortion pattern, compressible, steady state 3D-RANS simulations of the SE^{2}A blended wing body (BWB, Fig. 2)

reference design were conducted. The aircraft geometry and flight conditions are based on design studies carried out for the next design iteration of the BWB, as described in [7]. Nacelles designed following the methodology described in [8] were integrated onto the top rear of the aircraft fuselage. The DLR TAU-Code [9], a finite-volume-based Navier-Stokes solver is used for the CFD simulation, while the mesh is generated with CENTAUR. The mesh is unstructured except for prism layers in the near-wall regions. For turbulence modelling, the k-ω model is applied. The BWB is modeled as a half model with symmetry plane and all walls are considered viscous and adiabatic. A mass-flow boundary condition is applied at the engine intake and exhaust. Far-field conditions at the domain boundary are set to ISA conditions at the cruise operating point of the aircraft. The total pressure field at the nacelle inlet is then extracted and normalized with the far field total pressure p_{t0}. By generalizing the total pressure distortion with respect to the relative channel height, a transfer of the distortion pattern's shape to a different test case, with varying design conditions and main dimensions is possible.

Stage performance evaluation: To evaluate the aerodynamic performance of the fan stage, 3D stage passage simulations are conducted in Ansys CFX. For the rotor and stator domain with one blade each, a structured mesh is created with $y^+ = 1$ at all domain walls for the aerodynamic design point. A k-ω turbulence model is used and the speed lines are created by gradually increasing the static pressure at the domain outlet until numerical divergence indicates the numerical stability limit. For the consideration of BLI effects, the radial total pressure distortion p_t/p_{t0} is applied as a domain inlet condition.

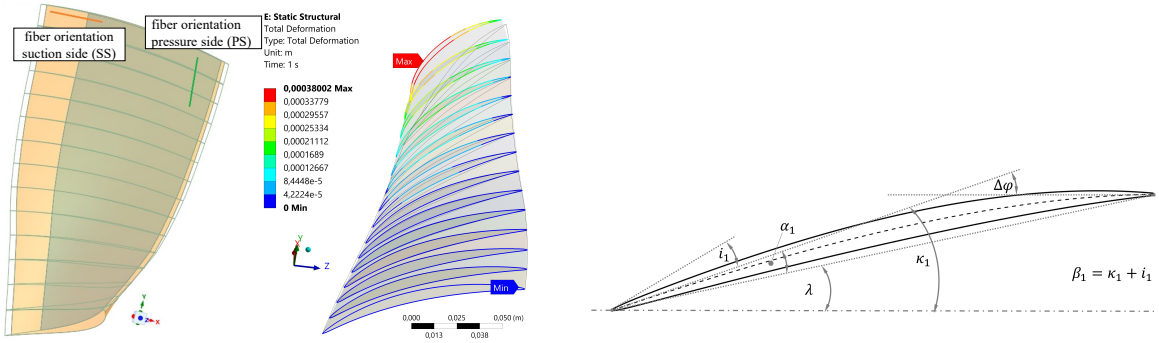

Figure 1: Actuator CAD models based on reference blade sections (left), simulated deformations at blade sections (center) and aerodynamic blade angle definition (right).

Structural morphing methodology: Mitigating the BLI induced drawbacks requires specific variations of the span-wise blade angles. After these requirements are derived from the CFD simulations, an angular optimization target for the structural design methodology is defined. Next to the morphing target the blade sections of the reference blade geometry are used to create a 3D CAD model of the blade (see Fig. 1). These sections also serve as a reference for the definition of the actuator geometry. After assigning material properties for the blading and the actuators, both geometries are meshed. Within this study, titanium is selected as the reference material for the blade body. The piezoceramic actuators are implemented as MFC actuators, as

described in [10]. The contact between actuators and blade is modeled with a contact bonding approach that allows to transfer the deformations from the actuators into the blade's structure. Through the introduction of an electric field, the actuators change their shape, leading to the blade's morphing. In the mechanical methodology the actuator's behavior is approximated with a simplifying thermal analogy. The analogy approximates the deformation that would normally be reached through the introduction of an electric field by defining suitable thermal boundary conditions. The aerodynamic reference sections are preserved throughout the entire morphing simulation to simplify the morphing evaluation and geometry engineering according to aerodynamic design and resolution requirements (Fig. 1, [4]). The structural morphing results are hence exported for the aerodynamic design sections. As displayed in Fig. 1, an extensive post processing routine transforms the directional displacement for every mesh node into a span-wise aerodynamic blade angle morphing, such as the variation of the leading edge metal angle

$$\Delta\kappa_1(r) = \kappa_{1,\mathrm{def}}(r) - \kappa_{1,\mathrm{ref}}(r) \quad \text{with} \quad \kappa_1(r) = \lambda(r) + \alpha_1(r) \quad , \tag{1}$$

where *def* refers to the morphed shape and *ref* to the blade angles of the reference geometry. The variation of the blade turning is calculated as follows:

$$\Delta\Delta\varphi(r) = \Delta\varphi_{\mathrm{def}}(r) - \Delta\varphi_{\mathrm{ref}}(r) \tag{2}$$

Blade design: For the design variations, streamline curvature (SLC) design calculations are conducted. By choosing a vortex design for the rotor design, the SLC procedure allows to estimate the meridional distribution of relevant flow quantities, defining the inflow as well as outflow angles of the rotor. Based on those, a suitable rotor geometry is derived and transferred to the structural morphing analysis. An efficiency evaluation based on [11] allows to iteratively assess the enthalpy rise through the rotor to achieve the required design point for a pre-selected mass-flow. The profile sections are defined with an equal spacing in span-wise direction. The main dimensions that determine the meridional shape of the blade, are the hub-to-tip ratio ν_{ht} that defines the blade length in radial direction and the aspect ratio AR that – with the hub to tip ratio fixed – yields the chord length c of the rotor. By selecting a maximum camber position and deriving the relative flow angles, where the meridional sections intersect with the leading and trailing edge of the rotor blade, the camber of the respective blade profile is modeled. Within this research a parabolic mean camber is combined with a thickness distribution defined through the Class Shape Function methodology [12]. The NASA rotor 67 reference shape is based on the original CSM approach, that yields a small leading edge thickness for transonic profile designs. For the design variations wedge shaped profiles, commonly used for transonic inflow conditions, are chosen, by relying on a thickness modelling extension, introduced by [13] (Fig. 6). This methodology allows to specifically adapt the leading edge thickness as well as the suction side curvature to control pre-shock flow acceleration and with that shock losses. For the implementation of lean and sweep, the sweep (ϕ_h, ϕ_s) and lean (ν_h, ν_s) angles are defined at the hub and shroud following [14]. The respective angles are then used to create a circular arc between hub and shroud that defines the span-wise stacking line. Depending on the radial blade position, the stacking line determines the respective profile displacement in their staggered chord direction (sweep) or perpendicular (lean) to it.

3 RESULTS

3.1 Impact of BLI on stage performance

Three speed lines at 100 %, 85 % and 70 % design speed are evaluated for an undistorted blade passage and a distorted blade passage, located above the fuselage (Fig. 2, right). There the isentropic efficiency η_{isen} (dashed) and the pressure ratio PR (solid) are displayed, depending on the absolute mass-flow $\dot{m}_{abs}$ through the stage.

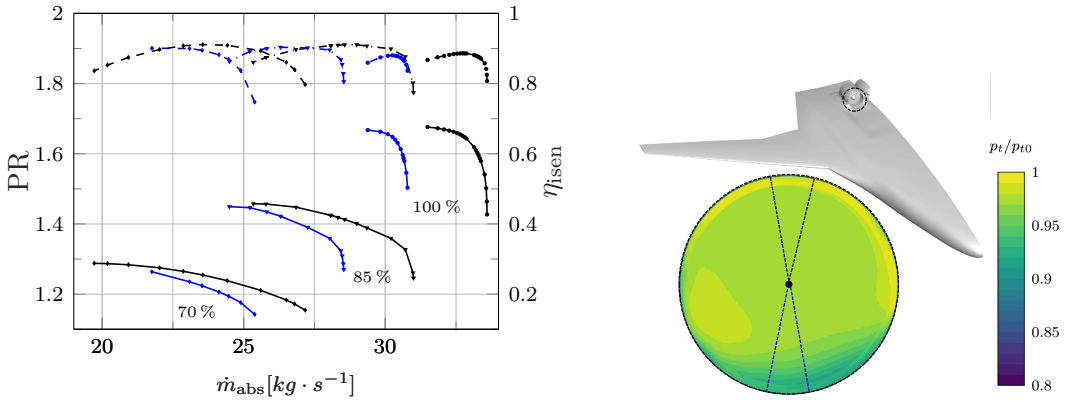

Figure 2: Left: Performance of the reference NASA rotor 67 with upstream distortion (blue) and undistorted inflow (black). Right: BWB half model with total pressure distortion pattern due to boundary layer ingestion.

Through the total pressure deficit upstream of the rotor, the achievable stage pressure ratio is decreased. This results in an increased loading of the rotor, combined with a reduced absolute mass-flow through the stage. Under distorted inflow conditions, the characteristic increase in tip loading under part load conditions becomes more critical, which results in the surge margin reduction for all speed lines displayed in Fig. 2. The deficit in design point mass-flow is highest for the 100 % speed line, as the rotor performance is highly sensitive towards the unique incidence condition (u.i.). Although the inlet distortion reduces the relative inflow Mach number, the inflow condition remains transonic in the upper flow regimes of the rotor. With a passage shock occurring in the upper flow regimes of the rotor, BLI mainly affects the u.i. condition and its characteristic mass-flow. With that, flow separation within the blade passage is mainly driven by the strength and position of the passage shock. A similar effect is visible for the right branch of the 85 % speed line, where the dependency on the unique incidence condition accelerates the mass-flow deficit. With a further reduction of the mass-flow a reduced percentage of the rotor operates under the unique incidence condition. With that the rotor performance is increasingly affected through flow incidence and the earlier onset of flow separation in the blade passage. The combination of raised blade loading and earlier flow separation are the dominant effects for the 70 % speed line, where the reduction in surge margin is strongest. A significant passage shock only occurs in the upper 15 % of the rotor, when the stage operates close to its choke limit, which leads to the higher mass-flow deficit towards increased operating mass-flows. For all speed

lines the achievable peak efficiency is reduced through the distorted inflow. With 1.15 % the efficiency deficit is highest for the 70 % speed line, driven by the increased flow incidence. For higher relative inflow Mach numbers, the BLI effect is dampened by the occurrence of a passage shock resulting in a lower peak efficiency deficit of 0.65 % for the 100 % speed line (Fig. 2, left).

3.2 Rotor morphing results

While the lower design point mass-flow is less critical for a BLI fan, the reduced surge margin and the decreased efficiencies need to be addressed in order to maintain a safe and efficient operation, especially during transient maneuvers and off-design operation. Both effects are driven by the flow incidence in the distorted fractions of the rotor. By temporarily increasing the leading edge metal angle, when the blade passes through the distorted flow regimes, shape adaption aims to dampen the drawbacks of BLI. An increase of the leading edge metal angle κ_1 is either possible through a stronger blade staggering λ or through a higher blade leading edge camber angle α_1 (Fig. 1, right). For both approaches, a suitable actuator configuration is determined. Fig. 3 shows the radial variation of the metal angle $\Delta\kappa_1$, the profile turning $\Delta\Delta\varphi$ and the blade staggering $\Delta\lambda$ for both actuator configurations, depending on the relative leading edge position r_{LE}.

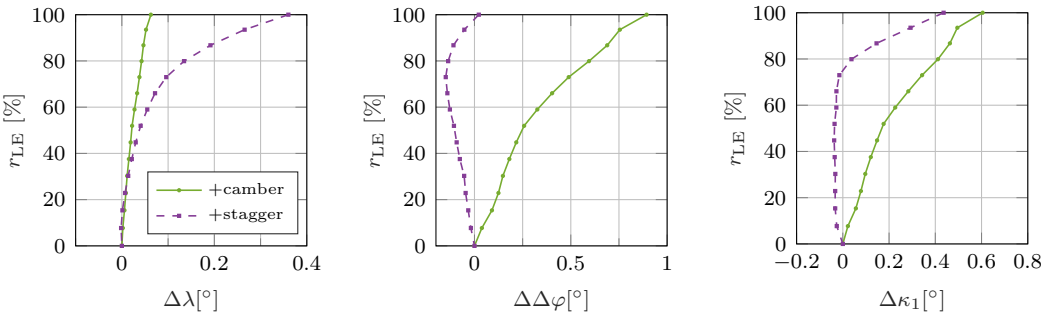

Figure 3: Achievable shape morphing for a stagger and a leading edge camber angle optimization.

Through the centered location of maximum thickness and camber position, an increase of the leading edge camber angle requires actuators that maximize the blade turning. With the fiber orientation determining the actuation direction and the cantilever of the forces applied into the blading, the structural design yields a fiber orientation that approximates the streamline slope of the tip section. This results in a fiber orientation of 2° for the suction side and 6° for the pressure side (see Table 1). Through a dominant expansion of the suction side actuator and a supporting contraction of the pressure side actuator, an increase of the blade turning by a maximum of 0.89° at the blade tip is achieved. The morphing of the stagger angle $\Delta\lambda$ with a maximum of 0.06° is however negligible compared to the dominant turning adaption. This results in a maximum incidence correction of $\Delta\kappa_1 = 0.61°$ at the blade tip.

With increasing fiber angles, the impact of the actuation on the blade turning is reduced and the blade staggering is increasingly affected. Depending on the blade aspect ratio, the structural design for an improved stagger angle morphing yields a fiber orientation of 51° for the suction side and 50° for the pressure side. An expansion of both actuators results in an increase

Table 1: Details for the applied actuator configurations.

	actuators	orientation (PS)	mode (PS)	orientation (SS)	mode (SS)
+camber	2	6°	expansion	3°	contraction
+stagger	2	50°	expansion	51°	expansion

of the stagger angle by 0.36° at the blade tip. The adaption of the blade turning remains below 0.2° with a local turning reduction maximum at 72 % blade height. This determines a leading edge metal angle adaption maximum of 0.42° at the blade tip. For the stagger adaption scenario, the achievable leading edge metal angle variation is concentrated in the upper 30 % of the blade. Contrarely, the κ_1 morphing for the first scenario extends towards the blade's root with significant deformation effects already occurring above 50 % blade height.

3.3 Improvement potential through shape adaption

A higher profile turning of the rotor through the *+camber* actuator configuration locally increases blade loading (Fig. 4). Under part load operation, the characteristic load redistribution towards the upper blade fraction is amplified, which improves the overall pressure ratio, but also provokes a reduction of surge margin as flow diffusion is accelerated. Through the increment in leading edge metal angle, flow incidence is reduced for those fractions of the rotor, which operate with the leading edge bow shock detached. As the radial fraction of the rotor that operates outside of the unique incidence condition increases towards the surge limit, a slight improvement of the stage efficiencies with reduced mass-flows is visible for the 100 % speed line. For lower design speeds, the increased pressure ratios and isentropic efficiencies become the dominant effect of the shape morphing, as the dependency on the unique incidence condition is less prominent. For the 70 % speed line, the relative inflow Mach numbers become too small for the unique incidence condition to have a significant influence on the overall performance variation, which results in a slightly elevated speed line compared to the distorted reference shape. For 100 % and 85 % design speed, the speed line variation towards the choke mass-flow is dominated by the shock occurring in the blade passage. According to the unique incidence condition, an increase in leading edge metal angle reduces the mass-flow through the passage, leading to the sinistral shift of the speed line visible in Figure 4. Additionally, the higher leading edge metal angle and overall blade turning correlates with an increase in suction side curvature. The occuring shock pattern is highly sensitive to increments in suction side curvature, as pre-shock flow is accelerated, which results in an elevated shock strength and higher shock losses. The resulting reduction of the stage efficiencies is especially dominant for the 100 % speed line.

An increase of the stagger angle (*+stagger*-scenario) constantly shifts the speed lines towards lower mass-flows. The higher leading edge metal angle either alters the unique incidence mass-flow for high flow coefficients and rotational velocities or allows for an incidence correction, in case the majority of the blade span operates with subsonic inflow or a detached leading edge bow shock. Through a slight reduction of the overall blade turning between 40 % and 90 % blade height, the achievable pressure ratios are lower for all operating points. The combination of a reduced blade loading with an incidence correction for lower design point mass-flows contributes to a slight increase in surge margin for all speed lines. Additionally, the overall efficiency is

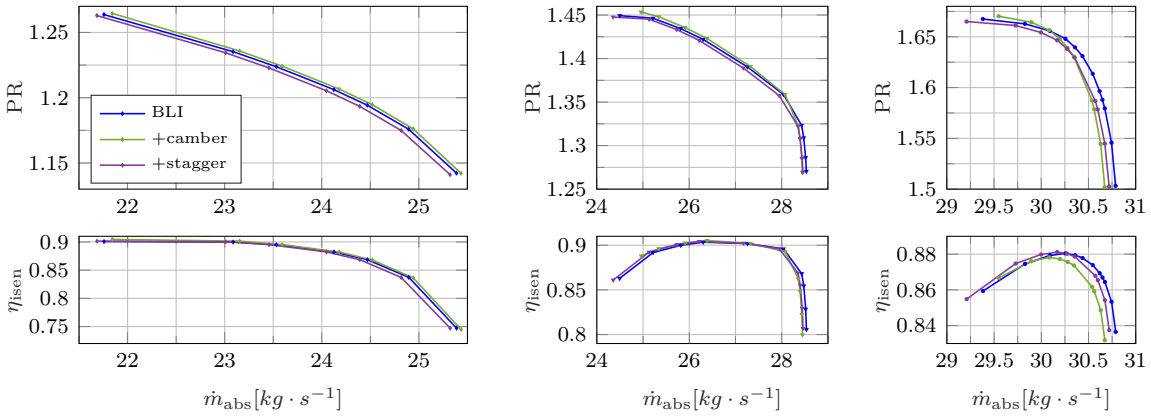

Figure 4: Impact of shape adaption on the stage performance at 70 % (left), 85 % (center) and 100 % (right) design speed.

improved. Towards the choke limit of the 100 % and 85 % speed lines, the reduced suction side curvature through the lower blade turning is the dominant effect, while the performance under part load conditions towards lower mass-flows benefits from the incidence correction that is achieved by the adaption of the stagger angle. For the 70 % speed line the improvement in isentropic efficiency is less distinct, as the achievable metal angle morphing is too small to alter the largely subsonic blade passage flow. The limitation of the effective stagger angle morphing for the *+stagger* scenario to the upper 30 % of the rotor further decreases its improvement potential for a fan rotor under distorted inflow.

3.4 Design adaption

Although the improvement potential of shape-adaption on a transonic compressor stage under BLI conditions becomes apparent, the achievable deformations are too small to significantly alter the drawbacks of ingesting low momentum fluid. With the actuator strength being limited, the blade shape remains as a design parameter for increasing the shape morphing potential.

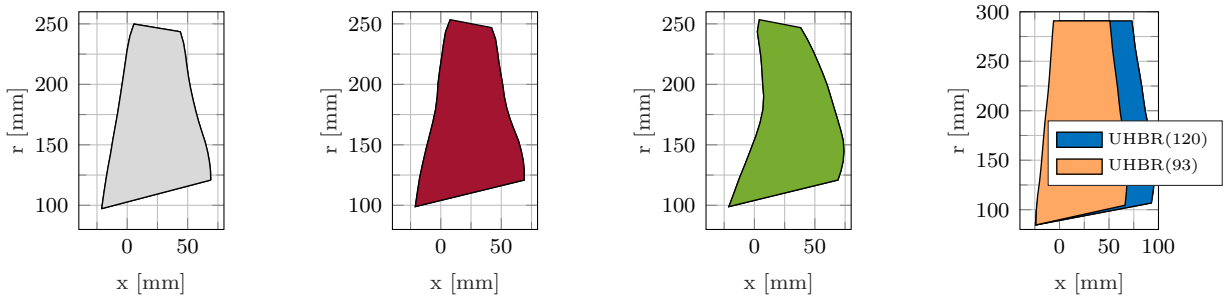

Figure 5: Design adaptions: (1) reference, (2) transonic, (3) lean/sweep, (4) UHBR.

Transonic re-design: With the goal of evaluating the impact of the detailed blade design on the shape morphing potential of the reference rotor, a re-design of the original NASA rotor

67 profiles is conducted. Using an extended CSM modelling approach, a wedge shaped profile prototype is created for the tip sections, which is then gradually merged into the subsonic profile shapes used for the lower 30 % of the rotor (Fig. 6). To maintain aerodynamic comparability with the reference design, the profiles are modelled for the same meridional stream lines. For the transonic blade re-design the leading edge thickness, the leading edge metal angle and the effective pressure side turning of the reference NASA rotor 67 are defined as design constraints. Through the pre-defined metal angle κ_1, the leading edge camber angle α_1 defines the span-wise blade staggering. This increases the blade twist, leading to a maximum reduction of the throat area by 11 % at the blade tip (Fig. 5 (2)).

Lean and sweep: A combination of lean and sweep is chosen for the 3D re-design. For both end-walls a positive sweep is selected with $\Phi_h = 10°$ at the hub and $\Phi_s = 30°$ at the shroud. Through the forward sweep at the blade tip lower relative inflow Mach numbers, and therefore a reduction of the shock losses can be achieved. The positive sweep at the blade hub section aims at an alteration of radial secondary flow phenomena and as a result at a reduction of end-wall losses. The swept configuration is combined with a positive lean, at the shroud ($\nu_s = 15°$) and the hub ($\nu_s = 20°$). Such a design alteration evokes a span-wise load re-distribution, while the occurrence of corner separation is mitigated (Fig. 5 (3)).

Scaled UHBR: Based on recent fan designs a lower hub-to-tip ratio ν_{ht} of 0.29 is selected, which increases the blade length by 25 %. This requires a reduction of the rotational speed, resulting in a tip Mach number of 1.05. For a suitable aerodynamic design, the design point pressure ratio is altered to $PR = 1.36$, while the design point mass-flow is increased to $\dot{m}_{\mathrm{DP}} = 48\ kg\ s^{-1}$. The increased blade length requires a reduction of the hub turning, resulting in a higher tip loading of the rotor design (Fig. 5 (4, orange)). In a second re-design, the chord length of the UHBR design is increased to allow for larger actuators (Fig. 5 (4, blue)). For the radial distribution of leading edge, trailing edge and maximum thickness the thickness-to-chord ratio $t\ c^{-1}$ of the original NASA rotor 67 is maintained, elevating the absolute thickness values for longer profiles. This design decision results from structural integrity requirements during operation.

3.5 Influence of design alterations on morphing potential

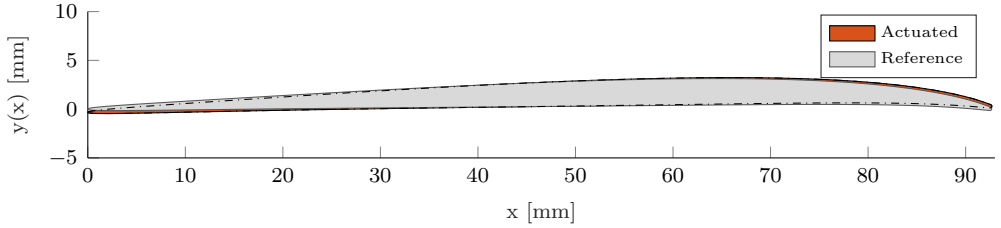

Figure 6: Tip section morphing for transonic re-design, relative to unstaggered design position.

For all design alterations, the *+stagger* actuator configuration displayed in Table 1 is applied,

keeping its fiber orientation, actuation mechanism and relative actuator width constant. This increases the actuator length, in case a wider chord is applied. The height and shape of the actuators is defined through the blade shape and the blade length, as all actuators extend from hub to blade tip. In Figure 7, the impact of the blade design on the span-wise morphing of the stagger angle $\Delta\lambda$, the blade turning $\Delta\Delta\varphi$ and the leading edge metal angle $\Delta\kappa_1$ for the *+stagger* actuator configuration is displayed.

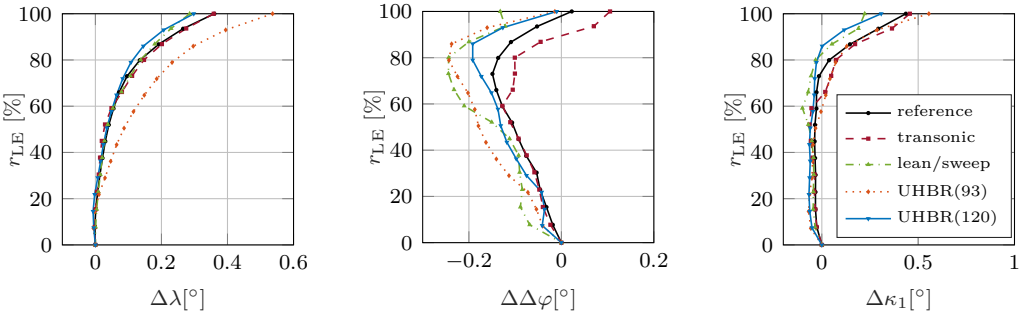

Figure 7: Impact of the blade re-design on the blade angle morphing for the *+stagger* scenario.

By relying on wedge shaped profiles in the transonic flow regimes of the rotor, the overall achievable leading edge metal angle morphing is increased above 60 % blade height compared to the reference blade design (Fig. 6). A similar improvement is achieved for the UHBR(93) re-design. While the UHBR morphing improvement results from a significant increase in stagger angle morphing (0.54°, see Fig. 7), the increased deformability of the transonic re-design results in an increased blade turning towards the blade tip. The UHBR(93) re-design even shows a reduced blade turning adaption, which dampens the overall stagger angle morphing effect on the leading edge metal angle variation. The UHBR design with an increased chord length and an application of lean and sweep reduces the feasible stagger angle morphing for the selected actuator configuration. For both design adaptions, a lower stagger angle morphing capability is paired with a turning angle reduction below 90 % blade height.

4 DISCUSSION

To mitigate the drawbacks of BLI on a blade passing through the distorted flow regimes of the rotor annulus, the increment in surge margin through a higher blade staggering is a promising approach. For a shape adaptive BLI fan, provoking a reduced resistance towards a stagger angle adaptability should therefore be considered. Although a higher blade turning offers an efficiency improvement for low transonic and subsonic inflow conditions, its secondary effect to reduce the surge margin is disadvantageous. However, combining the dominant stagger morphing with a subordinate increase in blade turning, could further improve the fan operation under BLI conditions. By mitigating the peak efficiency deficit through an incidence correction and a higher blade turning, fan efficiency could especially be improved under part load conditions. Within the transonic re-design that is used for all design adaptions, the CSM modelling extension is applied, which allows to increase the leading edge thickness according to the original geometry defined by Hathaway [3]. This increases the resistance of the blade against the piezoceramic

actuation, leading to a lower morphing potential. The lower hub-to-tip ratio of the UHBR re-design compensates that effect and allows a similar deformability compared to the reference design which exhibits a lower leading edge thickness in the tip region. The lower hub-to-tip ratio enables larger actuators, which exhibit an increase in cantilever for the forces applied into the blading through the piezoceramic actuation. This results in the significant increase in stagger angle morphing displayed in Fig. 7. Due to constraints imposed by the structural integrity requirements of the rotor blading, the leading edge thickness as well as the maximum thickness are defined as a percentage of the chord length. A further increase of the chord length leads to more material that needs to be displaced by the actuators and hence a higher resistance of the UHBR blading with a longer chord. This effect becomes especially apparent in Fig. 7, despite the larger actuators. Compared to the original profile shapes, where maximum thickness and camber position are located near 50 % of the blade length, the wedge shape of the transonic re-designs yields a slender contouring towards the leading edge. This boosts deformability in the leading edge area, facilitating a frontward shift of the maximum camber position through the piezoceramic actuation (Fig. 6). The resulting reduction in overall blade turning is strongest for the UHBR re-designs and the design variation with lean and sweep.

5 CONCLUSION

By ingesting the boundary layer of a blended wing body aircraft, the fan stage mass-flow is reduced and the loading of the fan rotor blading increases. The upstream total pressure deficit causes flow incidence and deviation due to the increased pressure rise requirement of each rotor blade that passes through the distortion. To mitigate those effects and to provide a sufficient surge margin, the rotor blading is morphed through piezoceramic actuators, while passing through the distorted flow regime. A morphing towards an increased blade staggering has indicated to improve the surge margin, while an elevated blade turning improves part load efficiency. A dominant stagger angle morphing, combined with a slight increase of the blade turning is therefore expected to show the highest potential for mitigating the BLI effects. The stagger angle morphing capability is however limited to a maximum of 0.36° and to the upper 30 % of the blade-span for the chosen CSM re-design of the NASA rotor 67. To improve the stagger morphing capability of a shape-adaptive BLI rotor, a re-design study was conducted. While a transonic re-design of the upper 60 % of the rotor shifts the maximum deformations towards the leading edge, a reduced hub-to-tip ratio and a higher blade aspect ratio lead to a significant increase in blade stagger angle morphing. Additionally, the achievable deformations extend further towards the blade root, improving the feasible extent of span-wise incidence correction. Although, the potential of shape adaption for mitigating the drawbacks of ingesting low momentum boundary layer fluid have been demonstrated within this research, the shape morphing potential requires improvement in order to further extend the stagger morphing capability. Based on the preliminary shape variation study, further adaptions of the blade reference shape need to be investigated, also including a variation of the actuation concept.

Acknowledgements: We would like to acknowledge the funding by the Deutsche Forschungsgemeinschaft (DFG, German Research Foundation) under Germany´s Excellence Strategy – EXC 2163/1- Sustainable and Energy Efficient Aviation – Project-ID 390881007.

References

[1] L. H. Smith, "Wake ingestion propulsion benefit," *Journal of Propulsion and Power*, vol. 9, no. 1, pp. 74–82. [Online]. Available: http://arc.aiaa.org/doi/10.2514/3.11487

[2] D. Giesecke and J. Friedrichs, "Aerodynamic comparison between circumferential and wing-embedded inlet distortion for an ultra-high bypass ratio fan stage," in *Volume 2A: Turbomachinery*. American Society of Mechanical Engineers, 06172019.

[3] M. D. Hathaway, "Unsteady flows in a single-stage transonic axial-flow fan stator row," Retrospective Theses and Dissertations, Iowa State University, Ames, 1986.

[4] M. Seidler, Z. Montano, J. Friedrichs, and J. Riemenschneider, Eds., *Introduction and Evaluation of an Aerostructural Coupling Approach for the Design of Shape Adaptive Compressor Blading*, ser. Proceedings of ISABE 2022, 2022.

[5] Smart Material GmbH, "Mfc engineering properties." [Online]. Available: https://www.smart-material.com/MFC-product-propertiesV2.html

[6] J. Voigt and J. Friedrichs, "Development of a multi-segment parallel compressor model for a boundary layer ingesting fuselage fan stage," *Energies*, vol. 14, no. 18, p. 5746.

[7] S. Karpuk, Y. Liu, and A. Elham, "Multi-fidelity design optimization of a long-range blended wing body aircraft with new airframe technologies," *Aerospace*, vol. 7, 2020.

[8] L. Benjamin, C. Heykena, J. Friedrichs, and C. Marquez, "Design and optimization of a nacelle for a uhbr turbofan engine using a class shape transformation based parameterization," ser. Proceedings of Global Power & Propulsion Society. GPPS, 2020.

[9] D. Schwamborn, T. Gerhold, and R. Heinrich, "The dlr tau-code: Recent applications in research and industry," in *ECCOMAS CFD 2006 CONFERENCE*, 2006.

[10] R. B. Williams, D. J. Inman, M. R. Schultz, M. W. Hyer, and W. K. Wilkie, "Nonlinear tensile and shear behavior of macro fiber composite actuators," *Journal of Composite Materials*, vol. 38, no. 10, pp. 855–869, 2004.

[11] R. O. Bullock and I. A. Johnson, "Aerodynamic design of axial-flow compressors. nasa sp-36," Washington, D.C., United States.

[12] D. Giesecke, M. Bullert, J. Friedrichs, and U. Stark, "Optimization of high subsonic, high reynolds number axial compressor airfoil sections for increased operating range," *Proceedings of GPPS Forum*, no. 18, pp. 1–9, 2018.

[13] M. Seidler and J. Friedrichs, "Introduction of an improved axial compressor profile shape modelling approach for increased flexibility in transonic profile design," ser. Proceedings of Global Power & Propulsion Society. GPPS, 2022.

[14] T. Eggers, H. R. Kim, S. Bittner, J. Friedrichs, and J. R. Seume, "Aerodynamic and aeroelastic effects of design-based geometry variations on a low-pressure compressor," *International Journal of Turbomachinery, Propulsion and Power*, vol. 5, no. 4, p. 26, 2020.